Published in final edited form as:
J Am Soc Mass Spectrom. 2011 June ; 22(6): 997–1013. doi:10.1007/s13361-011-0117-9.

Electron Transfer Dissociation of Milk Oligosaccharides

Liang Han[1,2] and **Catherine E. Costello**[1,2,3,*]

[1]Center for Biomedical Mass Spectrometry, Boston, MA 02118-2646 USA

[2]Department of Chemistry, Boston University, Boston, MA 02118-2646 USA

[3]Department of Biochemistry, Boston University School of Medicine, Boston, MA 02118-2646 USA

Abstract

For structural identification of glycans, the classic collision-induced dissociation (CID) spectra are dominated by product ions that derived from glycosidic cleavages, which provide only sequence information. The peaks from cross-ring fragmentation are often absent or have very low abundances in such spectra. Electron transfer dissociation (ETD) is being applied to structural identification of carbohydrates for the first time, and results in some new and detailed information for glycan structural studies. A series of linear milk sugars was analyzed by a variety of fragmentation techniques such as MS/MS by CID and ETD, and MS^3 by sequential CID/CID, CID/ETD, and ETD/CID. In CID spectra, the detected peaks were mainly generated *via* glycosidic cleavages. By comparison, ETD generated various types of abundant cross-ring cleavage ions. These complementary cross-ring cleavages clarified the different linkage types and branching patterns of the representative milk sugar samples. The utilization of different MS^3 techniques made it possible to verify initial assignments and to detect the presence of multiple components in isobaric peaks. Fragment ion structures and pathways could be proposed to facilitate the interpretation of carbohydrate ETD spectra and the main mechanisms were investigated. ETD should contribute substantially to confident structural analysis of a wide variety of oligosaccharides.

Introduction

Carbohydrates participate in various biological processes. They are involved in diverse roles such as molecular recognition, cell-cell and cell-matrix interactions, energy generation, and modification of protein conformations. Carbohydrates also serve as markers for many disease states. Increasing evidence shows that numerous biological functions are closely related to specific carbohydrate structures [1–4]. However, when compared to structural determinations of linear peptides or nucleic acids, elucidation of carbohydrate structures presents a much greater challenge, since many stereoisomeric structures can be formed from a very limited number of monosaccharides. Primary structural study requires not only composition and sequence analysis, but also the assignment of branching, linkage, and anomeric configuration[5]. Due to its extreme complexity, carbohydrate structure analysis is still at an early stage of development.

*Correspondence to: Prof. Catherine E. Costello, Center for Biomedical Mass Spectrometry, Boston University School of Medicine, 670 Albany Street, Rm. 511, Boston, MA 02118-2646, tel: (617) 638-6490, fax: (617) 638-6491, cecmsms@bu.edu.

Supplementary Material
CID and ETD MS^2 and ETD/CID MS^3 spectra of milk oligosaccharides as permethylated derivatives of the native glycans, and as derivatives labeled at the reducing end with ^{18}O prior to permethylation.

Mass Spectrometry (MS) is one of the most important tools for the structural characterization of carbohydrates, as it offers high sensitivity and addresses the most frequent biological problems, particularly with respect to analytes of interest that are present as components of complex mixtures or in very small amounts. Tandem mass spectrometry (MS^n), including low- and high-energy collision-induced dissociation (CID), has proven to be a powerful means for carbohydrate structural identification [6–8]. Generally, glycans undergo two main types of cleavage upon CID: glycosidic cleavages resulting from the rupture between the two neighboring residues and cross-ring cleavages that involve the fragmentation of a sugar ring. The former provide information on composition and sequence, while the latter provide some details on the different linkage types. Internal fragments are generated upon the occurrence of two (or more) cleavages, either glycosidic or cross-ring, from more than one site in the molecule [3]. They may also provide useful structural information.

Although low-energy CID does produce some cross-ring cleavages in oligosaccharides, the abundance of fragments resulting from cross-ring cleavages is relatively low in such spectra [6]. By comparison, more structural information can be obtained from the cross-ring cleavages created by high energy CID [8]. Recently, several novel fragmentation techniques have been applied to the analysis of carbohydrates. Adamson *et al.* and Zhao *et al.* have investigated the application of electron capture dissociation (ECD) to both linear and branched oligosaccharides by utilizing Fourier Transform Ion Cyclotron Resonance Mass Spectrometers (FT-ICR) [9, 10]. They showed that cross-ring cleavages were the dominant fragmentation pathway in ECD spectra. Whereas ECD is applied in the positive ion mode for characterization of neutral glycans, electron detachment dissociation (EDD) generates fragmentation in the negative mode for analysing acidic glycans, and has been shown to be particularly useful for analysis of glycosaminoglycans (GAGs). Wolff, Amster *et al.* applied EDD to the analysis of GAGs and elucidated some mechanisms and pathways [11, 12]. Adamson and Hakansson also showed that EDD produces relatively abundant cross-ring cleavage ions for *N*-glycans and milk oligosaccharides [13].

High-energy CID is unavailable on many modern instruments. Other alternative fragmentation techniques, including ECD and EDD, are mostly limited to FT-ICR MS, but the cost and complexity of these instrument systems limit their availability. Electron transfer dissociation (ETD), a fragmentation technique very similar to ECD, was introduced by Syka *et al.* for peptide/protein fragmentation [14]. In addition to its compatibility with high-end instrumentation, ETD can be carried out in quadrupole ion trap mass spectrometers, which are widely available. During ETD, multiply-charged ions react with an anion radical (*e.g.*, fluoranthene), leading to the generation of both odd-and even-electron fragments and molecular species with lower charge states. In contrast to CID, which preferentially results in cleavage of the most labile bonds, ETD induces a gentle reaction pathway and initiates fragmentation of the precursor ions through transfer of an electron from the radical anion to the analyte, and hence serves as a complement to CID [15]. This technique has been successfully applied to investigations in proteomics and glycoproteomics, and has been shown to be especially useful for localizing post-translational modifications [16, 17], but so far, the use of ETD for structural studies of glycans has not been reported.

Ion trap instruments offer many significant advantages for glycan analysis. They have high sensitivity and the ability to select a particular parent ion, fragment it, detect the product ions, and then repeat the isolation/fragmentation process multiple times. In this way, they can provide additional information for addressing the difficult analytical problems presented by carbohydrate structures [18]. Dissociation of a fragment ion may generate new types of product ions that cannot be observed in the first-stage dissociation of the original precursor ion [19–23].

Extensive studies have revealed that protonated oligosaccharides mainly produce glycosidic cleavages, yielding sequence but not linkage information [24–26]. Many reports have shown that fragmentation of different metal-adducted oligosaccharides (Li^+, Na^+, Mg^{2+}, Ca^{2+}, *etc.*) resulted in more cross-ring cleavages in low energy CID [25–28]. Lebrilla and co-workers discussed the relationship between the metal size, sugar size, and fragment ion yield. Probably the metal ion binding to a ring oxygen localizes the oxygen's electrons and prohibits glycosidic bond cleavages and it therefore induces abundant cross-ring cleavages under CID or IRMPD conditions [26, 29].

The derivatization of oligosaccharides by permethylation remains an important tool for detailed investigation carbohydrate structures. First, it decreases the intermolecular hydrogen bonding, thereby increasing the sample volatility and thus the intensity of the ion signals [30]. Second, it stabilizes structures against the effects from the excess energy transferred during ionization procedures such as Matrix-Assisted Laser Desorption/ Ionization (MALDI) [19, 31]. Third, permethylation enhances the formation of diagnostic fragment ions and thereby increases the yield of useful structural information [32]. Fourth, it can eliminate the negative charge associated with acidic residues, and thus stabilize acidic residues in the positive mode; this feature is especially important for the analysis of sialylated glycans in which the carboxyl group is located on the same carbon as the glycosidic linkage [33].

Considering the limitations of classic fragmentation techniques in widely used instruments, we undertook an exploration of the potential for use of ETD, in conjunction with CID, for structural determinations on oligosaccharides. In the current study, a series of linear milk sugars ----- LNT, LNnT, LSTa, LSTb and LSTc ----- has been investigated by ETD performed in the AmaZon ion trap (Bruker Daltonics, Billerica, MA). Different metal salts were selected from alkali, alkaline earth, and transition groups, including Na^+, Li^+, Ca^{2+}, Mg^{2+}, and Zn^{2+}, and tested to determine which metal adducts provided the most informative fragmentation behavior under ETD conditions. The metal iron (Fe) was not investigated as it cannot easily form complexes with oligosaccharides [34]. In order to achieve unambiguous assignments of product ions, reduction and ^{18}O labeling were used in parallel to provide two different types of modification at the reducing end of each milk sugar. The further utilization of MS^3 techniques made it possible to verify many assignments and to distinguish isobaric peaks. A combination of these approaches was employed to investigate the major mechanisms in the fragmentation pathways and facilitated interpretation of the carbohydrate ETD spectra.

Experimental Section

Materials

Lacto-*N*-tetraose (LNT, Galβ1→3GlcNAcβ1→,3Galβ1→4Glc), lacto-*N*-neotetraose (LNnT,Galβ1→4GlcNAcβ1→3Galβ1→4Glc), LS Tetrasaccharide a (LSTa, Neu5Acα2→3Galβ1→3GlcNAcβ1→3Galβ1→4Glc), LS Tetrasaccharide b (LSTb, Galβ1→3(Neu5Acα2, →6)GlcNAcβ1→3Galβ1→4Glc) and LS Tetrasaccharide c (LSTc, Neu5Acα2→6Galβ1, →4GlcNAcβ1→3Galβ1, →4Glc) were generous gifts from D. S. Newburg. All salts, including sodium chloride, lithium acetate, calcium chloride, magnesium sulfate, zinc acetate dihydrate and other reagents were purchased from Sigma Chemical Co. (St. Louis, MO).

Sample preparation

^{18}O-labeling and reduction were used in parallel to modify the reducing end of each milk sugar. For ^{18}O-labeling, 2.7 mg of 2-aminopyridine was added into 1.0 mL of anhydrous MeOH to make the catalyst solution [21]. Each dry, native oligosaccharide (1 μg) was

dissolved in 20 μL of $H_2{}^{18}O$ (97%) and then 0.8 μL of AcOH and 1.5 μL of catalyst solution were added. The mixture was left at 40 °C for 16 h. The reducing ends of oligosaccharides were hydrolyzed and recyclized under the acidic conditions. $H_2{}^{18}O$ exchanged the anomeric hydroxyl group with ^{18}OH [35, 36]. Then the ^{18}O-labeled native samples were dried in a SpeedVac (Thermo-Fisher, Waltham, MA) and were then ready for permethylation. The ^{18}O-labeling experimental conditions were deliberately adjusted to achieve a 1:1 $^{16}O/^{18}O$ ratio so that the spectra would display a 1:1 doublet for the $^{16}O/^{18}O$ species. For these derivatized mixtures, the fragment ions retaining the reducing end show both ^{16}O and ^{18}O product ions, while those retaining the non-reducing end do not: these differences validate the assignments of product ions. For simplicity and due to space constraints, the fragment ion peaks in these spectra are labeled only with the *m/z* values observed for the ^{18}O-labelled species. The spectra of the pure ^{16}O species appear in the Supplementary Material and may be used for comparison. To prepare the reduced glycans, a second set of the samples was treated according to the protocol reported by Costello and Cipollo [37]. Both the ^{18}O-labelled and the reduced samples were subjected to permethylation before mass spectral analysis.

The native and derivatized oligosaccharides were permethylated using the procedure of Ciucanu and Kerek [38], as improved by Ciucanu and Costello [39]. The permethylated oligosaccharide samples were each purified using a C-18 Ziptip (Millipore Corp., Billerica, MA) and were desalted twice. Then the samples were dissolved in 50/50 methanol/water to a concentration of 0.5 pmol/μL. The final concentration of metal salts was 2–5 μM.

Instrumentation

All experiments were performed with an AmaZon ETD Ion Trap mass spectrometer (Bruker Daltonics, Billerica, MA). Samples were infused via the Apollo II electrospray ion source equipped with dual funnel transfer, at the flow rate of 100 μL/h. Enhanced resolution mode was used with the scan speed of 8100 *m/z*/sec. The sample cations were transferred through the octopole and captured in the High Capacity Ion Trap. Anion radicals of fluoranthene were generated in the negative Chemical Ionization source (nCI source), transferred into the ion trap and then reacted with multiply-charged cations (*i.e.*, ion/ion reactions). The parameter settings for positive-ion ESI-MS were as follows: capillary voltage, −4500 V; end plate offset, −500 V; nebulizer, 4 psi; dry gas, 2 L/min; dry gas temperature, 150 °C. The amplitude of the voltage for CID MS/MS was typically 0.3–0.8 V. For ETD MS/MS, the maximum accumulation time of fluoranthene anions was 20.0 ms. The “Remove” function was activated at 210.0 Da to remove excessive fluoranthene anions. The reaction time was typically 120–160 ms and the cutoff was 120–170 ms. The ICC ETD target was 200,000–300,000. The "Smart Decomposition" was set for 2 charge states. This function utilizes resonant excitation (but does not itself cause fragmentation) and performs a ramping of the voltage from 80% – 125% of the normal value for that *m/z* value, in order to overcome other attractive interactions (*e.g.*, hydrogen bonds/non-covalent forces) between fragments [40]. For MS^n experiments, the fragmentation parameters had to be altered significantly, due to the different features of product ions. Mass resolution was 7000–10,000. Mass accuracy was 100–200 ppm above *m/z* 400 and 200–500 ppm below *m/z* 400. The software used for data processing and interpretation was Compass DataAnalysis (Bruker Daltonics).

Results and Discussion

Five (a) permethylated, (b) reduced and permethylated, or (c) both labeled with ^{18}O at the reducing end and permethylated milk sugar samples, each cationized with Li^+, Na^+, Mg^{2+}, Ca^{2+}, or Zn^{2+} salts were subjected to electrospray ionization and fragmented in the AmaZon 3D ion trap. CID MS/MS, ETD MS/MS, CID/ETD MS^3 and ETD/CID MS^3 spectra were obtained. No $[M + Zn]^{2+}$ ions were detected in the MS spectra; this result indicates that Zn^{2+}

cannot form metal complexes with these sugars. In the ETD spectra of doubly-charged precursor ions $[M + 2Li]^{2+}$ and $[M + 2Na]^{2+}$, the corresponding charge-reduced species $[M + 2Li]^{+}\cdot$, $[M + 2Na]^{+}\cdot$ and the singly charged ions $[M + Metal]^{+}$ were accompanied by few fragment ions. In contrast, both Mg^{2+} and Ca^{2+} adducts generated both the charged-reduced $[M + Metal]^{+\cdot}$ and $[M + Metal - H]^{+}$ and more types of fragment ions under ETD conditions. Consistent with the report of Harvey [25], the order of sensitivity was $Ca^{2+}>Na^{+}>Mg^{2+}$. We observed that Ca^{2+} provided two to three times the sensitivity compared to Mg^{2+} (data not shown). In Ca^{2+} MS/MS spectra, we observed many glycosidic bond cleavages similar to Mg^{2+} spectra, but fewer cross-ring cleavages. Magnesium adducts provided a greater variety of fragment ions than did calcium adducts. After reduction or ^{18}O-labeling on the reducing end and permethylation, the X, Y and Z ions which retained the intact reducing end exhibited a shift of 16 Da or 2 Da, respectively, relative to the permethylated native samples. In this way, isobaric peaks, observed in the spectra of native oligosaccharides, that might contain either the reducing or non-reducing ends of the glycans, could be differentiated from one another on the basis of the occurrence of shifts in the spectra of the derivatives. Reduction and/or ^{18}O-labeling also provided many clues that facilitated making definitive assignments for most fragment ions in the CID and ETD spectra. Where necessary, MS^3 measurements were also carried out. The spectra of the reduced and permethylated samples adducted with magnesium salts provided the most valuable information that contributed to differentiation between isomers. Therefore, they will be discussed in detail in this paper. The CID data recorded for different derivatives and various cations exhibited high similarities with respect to the types of abundant ions, although they varied in the extent and types of the low abundance products that resulted from cross-ring cleavage. In order to avoid the repetitious presentation of similar information, the CID spectra of LNT and LSTa have been chosen to represent the typical fragmentation patterns for all CID spectra. Data obtained for the other glycans and for the derivatives not shown in the figures are available in the Supplementary Material. The nomenclature introduced by Domon and Costello has been used for designations of fragment ion assignments [41]. The ions that result from glycosidic cleavages have been labeled in red; those that originate from cross-ring cleavages have been labeled in blue, and those from internal glycosidic cleavages, with or without additional loss of neutrals, in green. The peaks labelled in purple represent doubly charged ions.

Figure 1 presents the CID MS/MS spectrum and the product ion assignments for the $[M + Mg]^{2+}$ ion formed *via* Mg^{2+} adduction to reduced and permethylated LNT, and Figure 2 shows the analogous ETD MS/MS spectrum and assignments. In the CID spectrum, the high abundance peaks can be attributed to glycosidic cleavages. The doubly-charged precursor ion $[M + Mg]^{2+}$ and the corresponding singly-charged ion $[M + Mg - H]^{+}$ were observed at *m/z* 471.7 and 942.5, respectively, the latter resulting from loss of a proton.

The ion observed at *m/z* 228.0, produced by the internal cleavages Z_3/B_2 on either side of the 1→3-linked GlcNAc residue in LNT as shown in the Figure 1a, does not appear in the corresponding CID spectrum of LNnT in which the GlcNAc is 1→4-linked (Figure 3); this is likely due to the difference in the position of the linkage between Gal1 and GlcNAc2 that determines when the basic nitrogen can participate in the elimination. Therefore, it can be referred as a diagnostic peak that can differentiate the isomers LNT and LNnT [20, 21]. We also detected doubly-charged product ions in the CID spectrum; these resulted from either glycosidic or cross-ring cleavages. The glycosidic cleavages furnish sequence information for glycans. The linkage information provided by the several cross-ring cleavages observed in the CID spectrum was not sufficient to specify the different linkage types.

In contrast, only singly-charged product ions were found in the ETD spectrum (Figure 2). Both $[M + Mg]^{+}\cdot$ at *m/z* 943.5 and $[M + Mg – H]^{+}$ at *m/z* 942.5, were observed in the ETD spectrum. As a indication that the gentle transfer process leads to relatively cool ions, the

spectrum includes a cluster that corresponds to addition of water to the singly-charged molecular species. In this and all ETD mass spectra of the permethylated glycans, abundant fragment ion peaks are formed by elimination of 15 u ($CH_3\cdot$) or 31 u ($CH_3O\cdot$) from the otherwise intact charge-reduced radical, and from odd-electron forms of the X_n- and Z_n-ions[42]. In addition to the products resulting from glycosidic cleavages, a substantial population of products derived *via* cross-ring cleavages was present, and these contributed supporting evidence for assignment of the linkage positions. Internal fragments were also found in the ETD spectra. C_3 and Z_3 ions were isobaric and could not be distinguished under the experimental conditions. However, the ETD/CID MS^3 spectrum obtained by selection of the ion at *m/z* 708.2 in the ETD MS/MS spectrum, followed by CID of this fragment, showed that there was a mixture of C_3 and Z_3 fragments (MS^3 data in Supplementary Material). The abundant peak at *m/z* 550.2/551.2 was formed by loss of CH_2CO or $CH_3CO\cdot$ from $^{2,5}X_2$. This type of fragment was found in all ETD spectra of glycans that had the [GlcNAc(1→3)Gal(1→4)Glc] moiety in each case. Subsequent losses of 15 u ($CH_3\cdot$) or 31 u ($CH_3O\cdot$) from the ion at *m/z* 550.2/551.2 were also observed. (It is quite possible that the $CH_3\cdot$ or $CH_3O\cdot$ loss occurs directly from $[M + Mg]^{+\cdot}$ prior to the cross-ring cleavage and ketene loss.) The fragment that corresponds to the loss of a methyl radical from the $^{2,5}X_2'$ ion is isobaric with the $^{0,2}X_2'$ species and the contribution from each will need to be explored at high resolution. (The reader should note that the sequence fragment symbol followed by a prime (') is used herein as it has been employed for carbohydrates, *i.e.*, to designate a species that has undergone loss of a neutral, and not as it has been used for peptide fragments where it signifies transfer of a hydrogen.) Extensive fragmentation occurred on the nonreducing end, whereas minimal fragmentation involved the reducing end. Comparison of the spectra of the native and ^{18}O-labeled glycans affirmed that few product ions resulted from fragmentation at the reducing end. The bulky groups at positions C_4, C_5 and the anomeric carbon from Gal1 are all oriented in the same direction, and thus form a suitable pocket to hold the magnesium cation. This could be one of factors that drive the occurrence of extensive ring cleavages.

Figure 3 shows the ETD spectrum of reduced and permethylated LNnT with Mg^{2+} adduction. All four kinds of fragment ions generated by glycosidic cleavages (B, C, Y and Z), cross-ring cleavages (A and X) and internal cleavages, can be observed in this ETD spectrum. It should be noted that a number of $[M + Mg - 71]^+$ or $[M + Mg - 73]^+$ product ions were detected due to the elimination of the group NCH_3Ac +/− H· under the ETD conditions. Both $B_2(H)$ and $B_2(Mg)$ were observed, at *m/z* 464.2 and *m/z* 488.2, respectively. The $B_2(H)$ ion originated from rupture of the glycosidic bond between GlcNAc2 and Gal3 and direct formation of an oxonium ion without attachment of a metal cation. $B_2(Mg)$, *m/z* 488.2, is a singly-charged even-electron species produced by electron transfer dissociation. Like all members of this series observed to date, it differs from the corresponding $B_n(H)$ ion by 24 u and thus contains an extra 2H. (Simple replacement of $2H^+$ with Mg^{2+} would yield a mass shift of 22 u, since the most abundant isotope of Mg has the atomic mass 23.99.) The ion at *m/z* 708.2 was attributable to both C_3 and Z_3, and both assignments were also supported by its ETD/CID MS^3 spectrum. It is worth noting that both Z_3 and $Z_3\cdot$ were observed in the ETD spectra of LNT and LNnT. The suggested structures for Z ions and B ions will be discussed later.

$^{1,4}A_3$ and $^{2,4}A_3$ product ions were present in the ETD spectra of both LNT and LNnT, indicating that there could be a 1→3 or 1→4 linkage between the GlcNAc2 and Gal3. No further information could be found in the ETD MS/MS spectra to permit assignment of the exact linkage type. LNT and LNnT only differ by the linkage between the Gal1 and GlcNAc2 residues. However, the fragment ions that arose from cleavages around the GlcNAc residue were the same in the two ETD spectra, although there were some differences in the relative abundances of the relevant product ions. The difference could not

be established solely on the basis of the information in the ETD MS/MS spectra. Therefore, the ETD product ions at *m/z* 738.2 were further explored with MS^3 experiments, using CID in order to differentiate the two isomers. Both of these ions could be attributed to internal cleavages (Figure 4a and 4b). The structures deduced from the MS^3 spectra are formed by loss of 2 x 102 Da from the two Gal residues; these were consistent with the presence of a 1→3 linkage between GlcNAc2 and Gal3. The peak which appears at *m/z* 534.2 in the LNT MS^3 spectrum was likely formed by elimination of the *N*-acetyl group and the residual Gal1 residue, leading to formation of a double bond. The presence of this ion further suggested that there had been a 1→3 linkage between GlcNAc2 and Gal1. In the MS^3 spectrum of LNnT, the occurrence of sequential losses from the GlcNAc residue hinted that there is a 1→4 linkage between GlcNAc and the non-reducing terminal Gal. The loss of methanol (32 Da) was an efficient process and was followed by elimination of $O{=}CH\text{-}CH_2\text{-}OCH_3$ (74 Da) and an $\cdot NCH_3CH{=}C{=}O$ group (72 Da), which can all be attributed to the presence of a 1→4 linkage.

LSTa

The study was extended to include larger milk sugar isomers having a sialic acid residue on the non-reducing end. Both CID and ETD were performed on the magnesium-adducted derivatives of LSTa. The resulting spectra are shown in Figures 5 and 6, respectively. Here also, glycosidic cleavage was the dominant fragmentation pathway in the CID spectrum, with few cross-ring cleavages being detected. The high abundances of the Y_4, $B_3(H)$ and $B_3(Mg)^{2+}$ ions could be ascribed to the proton affinity of the GalNAc residue. The internal cleavage ions originated from either glycosidic or cross-ring cleavages, as indicated in the scheme in Figure 5a. The information provided by the CID spectrum was limited and did not provide full definition of the complex structure.

By comparison, various types of ions arising from cross-ring fragmentations, combined with the glycosidic fragment ions observed in the ETD spectrum allowed confident assignments on the sequences and linkages of the monosaccharide residues. Two sequential losses of 102 Da from the intact molecule suggested the presence of at least two 1, 3 linkages, since this type of cleavage eliminates unsubstituted C4-C6. Within the sialic acid residue a number of cross-ring bond cleavages led to abundant fragments, *e.g. m/z* 1186.5, 1201.5, 1216.4, 1231.4 1243.5. The reason is likely related to the 3-dimensional structure of the sialic acid. The magnesium cation may prefer to bind with the multiple oxygen donors at the flexible chain extending from C_5 and may thus facilitate extensive fragmentation within the sialic acid residue. Additionally, $\cdot NCH_3Ac$ and $\cdot COOCH_3$ were both easily eliminated from the unit. As discussed above, losses of 71 or 73 Da correspond to elimination of NCH_3Ac +/- H· from the *N*-methyl, *N*-acetyl group (NMeAc).

As was observed in the spectra of LNT and LNnT, signals at *m/z* 550/551 were detected in the ETD spectrum of LSTa and could be assigned to $^{2,5}X_2'$ which contains the reducing end of the glycan. The presence of the $^{2,4}X_3$ and $^{2,4}A_3$ product ions suggested that the linkages between the sialic acid1 and Gal2, and between Gal2 and GlcNAc3 were either 1→3 or 1→4. However, there was little information to specify the linkage type between the GlcNAc3 and Gal4 residues. The ETD/CID MS^3 spectrum of *m/z* 1099.3 which corresponds to the $[M + Mg - H]^+$ of the product ion that resulted from the (2x102 Da) loss (Figure 7) indicated that they are all 1→3 linkages due to observation of the third loss of 102 Da, this time originating from the C_2 fragment.

LSTc

The ETD MS/MS spectrum of LSTc, depicted in Figure 8, was characterized by abundant cross-ring cleavages (A and X ions). The $^{3,5}X_3$, $^{0,4}X_3$ ions helped to identify the 2,6 linkage

between the Sialic Acid1 and the Gal2 residue. The signal at *m/z* 1099 was not detected in the spectrum of LSTc, further denoting the major structural difference of the linkage types from LSTa, in which there are three 1→3 linkages. The presence of product ions $^{3,5}A_3$, $^{0,3}A_3$ and $^{2,4}A_3$ demonstrated that there is a 1→4 linkage between GlcNAc3 and Gal2. Losses of the NMeAc group from both the sialic acid residue and the GlcNAc residue were also observed. The fragmentation on the sialic acid residue was very similar to that observed in the LSTa ETD spectrum. When the ETD spectrum of LSTc is compared to the ETD spectrum of LNnT, it can be seen that the presence of the sialic acid residue resulted in the appearance of more A ions that arise *via* fragmentation of the GlcNAc3 residue. This phenomenon can probably be attributed to the specific structure of sialic acid which prefers to bind metal and retain charges at the non-reducing side, as discussed above.

LSTb

LSTb was the only branched oligosaccharide included in the study set. In the ETD spectrum (Figure 9), the $^{2,5}X_2'$ peaks at *m/z* 550/551 Da were again observed. The appearance of $^{0,4}A_2$ was consistent with the presence of the 2,6 linkage between the 1α branch, Sialic Acid1, and Gal2. The linkage type between the terminal Gal1β and Gal2 can be verified by the presence of $^{0.3}A_2$ and $^{1,4}X_2$ fragments. All types of glycosidic cleavages were found, and these provided Figure 9. ETD MS/MS (a) fragmentation and (b) spectrum of reduced and permethylated LSTb $[M + Mg]^{2+}$ *m/z* 652.3. Fragments between *m/z* 1115.4 and 1216.4 are attributed to cleavages within the sialic acid residue. complete sequence information for the oligosaccharide. Fragments resulting from various internal cleavages were found in the ETD spectrum, such as $Y_{3\alpha}/Y_{3\beta}$, $C_2/Y_{3\alpha}$, $Y_{3\alpha}/Z_{3\beta}$, *etc*. Some of the fragment ions that originated from the terminal Gal1β were isobaric with fragments derived from the sialic acid residue. The assignments of these peaks could not be verified by MS^3 due to their very low abundances.

ETD Fragmentation mechanisms

ETD mechanisms have not previously been proposed for carbohydrates and their derivatives. In this study, "Smart Decomposition " was always utilized to increase fragmentation efficiency; this, however, makes definition of the fragmentation pathways even more complicated. It was applied after the ETD event and after the reagent ions were removed from the ion trap. Throughout the following discussion of the ETD spectra of glycans, the fragmentation pathway is presumed to involve influences from both ETD and CID. Several possible pathyways may generate the product ions: 1) A doubly-charged precursor ion takes up an electron that is transferred from an anion radical, leading to a singly-charged odd-electron ion such as $[M + Mg]^{+\bullet}$ (or its decomposition product that results from elimination of one or more neutral fragments), or a singly charged even-electron ion, resulting from the loss of a hydrogen radical $[M + Mg - H^{\bullet}]^+$ or larger radical $[M + Mg - R^{\bullet}]^+$. 2) The doubly-charged precursor ion can undergo electron transfer without dissociation of the resulting products (ETnoD), due to the persistence of non-covalent interactions which are sufficiently strong to prevent separation of the product ions [43]. When such a "wounded but intact" molecular cluster is subsequently subjected to CID conditions, the process leads to separation of the odd/even product ions that had been generated in the first encounter but held together through salt bridges or other noncovalent interactions. 3) Additionally, the doubly-charged precursor ion can lose a proton to form $[M + Mg - H^+]^+$, a species which is detectable in all the ETD spectra shown here, and then this may be neutralized by further electron transfer or fragmented upon collision-induced dissociation. The occurrence of these multiple processes correlates with the observation that the overall signal intensity in ETD spectra represents a 10-fold decrease compared to that from the corresponding CID spectra recorded under the same conditions (See Scheme 1). It should be kept in mind that the resolving power of the instrument, although high for a QIT,

is not sufficient to separate an electron transfer reaction followed by dissociation of a hydrogen atom from a proton transfer reaction.

In order to elucidate the mechanism(s) in the ETD pathway, metal coordination also needs to be considered. Linear peptides can undergo several types of coordination with metal ions. However, the possibilities for interactions of oligosaccharides and metals are broader, due to their complex structures [28]. Metal coordination will change the configurations of carbohydrates, leading to multiple dissociation mechanisms [44]. The groups of Lebrilla and Leary have studied [26, 29, 45] the binding sites of different metals to oligosaccharides utilizing the CID technique, and have thus provided valuable background information for the studies reported herein. Metal ions generally coordinate with several glycan oxygen atoms simultaneously [28, 29]. The most highly preferred binding position for alkali (*e.g.*, Na^+, Li^+) and alkaline earth (*e.g.*, Ca^{2+}) metal ions is the pocket between two adjacent sugar rings in one oligosaccharide molecule; this means the metal can coordinate with both the oxygen in the glycosidic ring and with the oxygen in the C-6 hydroxyl group [26, 29]. The ionic radius of magnesium is small (0.65 Å) and it can easily fit within other sites around the oligosaccharide. This could be one of the reasons that a larger number of product ions were found in the ETD MS/MS spectra of glycan-Mg^{2+} adducts, than were seen in the ETD MS/MS spectra of glycan-Ca^{2+} adducts. The relatively bulky calcium ion may be restricted in its binding sites to oligosaccharides due to its larger ionic radius (0.99 Å); this property may cause less distortion of the original structure, stabilize the adduct and decrease the dissociation yield [28].

In the CID spectra of the studied milk oligosaccharides, several doubly-charged product ions resulted from either glycosidic or cross-ring bond cleavages. In ETD spectra, however, all ions were detected as singly-charged odd/even species and they were not simply charge-reduced ions. Obviously, they were generated by mechanisms different from well-defined CID mechanisms. As the ETD fragmentation mechanisms are elucidated, they are being found to involve radical-initiated reactions, accompanied by hydrogen transfer and rearrangements. Since the simultaneous breaking of two bonds seems unlikely under ETD conditions, a stepwise mechanism would appear to be more appropriate as an explanation for the formation of the observed products. The routes to formation of C-ions and Y-ions can be expected to be similar. The anion radical will transfer the electron to the glycosidic oxygen, thus rupturing the glycosidic bond and leaving a radical on the adjacent carbon. The metal cations prefer binding to the oxygen anion, resulting in the generation of C- or Y-type product ions and a radical. (Schemes 2, 3).

For Z ions, both singly-charged odd-electron species and even-electron species were detected. The appearance of singly-charged Z ions in the ETD spectra and their absence in the CID spectra indicates the occurrence of radical-driven fragmentation accompanied with radical mobility and hydrogen migration. One possible route is the formation of a double bond after the rupture of the glycosidic bond, leading to the singly-charged, even-electron species and a radical (Scheme 4a). In this mechanism, both hydrogen migration and rearrangement are involved, and these will result in a singly-charged odd electron species and a neutral product, as shown in Scheme 4b. Wolff *et al.* speculated that the excess energy deposited into the ion during electron irradiation in EDD can supply the energy necessary to drive the observed hydrogen rearrangements [12]. Although the energies involved are lower, a similar case may occur in ETD.

B-type ions are observed as singly-charged species associated with either (H) or (Mg). The most abundant isotope of Mg weighs 23.989 and the metal carries a charge of 2^+. Although the peak assigned to the doubly-charged (Mg) species corresponds to a simple exchange of Mg^{2+} for $2H^+$ (Figs. 1 and 5), the singly-charged (Mg) species must represent B_n(Mg)+2H

since this series appears 24 u above the corresponding member of the B(H) series and 16 u below the corresponding member of the C_n series (Figs. 2, 3, 6).

The fragmentation pathways and mechanisms for formation of the cross-ring cleavages may be similar to the glycosidic cleavages. Routes that could generate the most common types of cross-ring cleavages are illustrated in Schemes 6–8.

However, there could be other possible explanations for cross-ring cleavages, such as Electron Transfer with no Dissociation followed by Collision-Induced Dissociation (ETnoD-CID) when "Smart Decomposition" is applied. Electron transfer to the precursor ion is expected to decrease the overall activation barrier in the whole system. Then, the "Smart Decomposition" can rupture the weakest bonds on the glycan rings followed by CID-induced pericyclic retro-aldol and retro-ene mechanisms [8] with the charge retained on either the non-reducing or reducing end, leading to formation of A or X ions, respectively. CID, as either a first or second dissociation stage, can result in retro-Diels Alder fragmentations of the rings and to multiple neutral losses of methanol (32 Da), ketene (42 Da), ethanol (46 Da), and larger species from the permethylated glycans, as indicated on the spectra shown in the figures.

Conclusions

The utility of ETD has been demonstrated for characterizing a series of milk sugars and defining fragments that distinguish one from another. In this first phase of the research on the electron transfer dissociation of glycans, we utilized simple, linear or minimally branched milk sugar isomers to investigate ETD pathways in carbohydrates. Generation of cross-ring cleavages was found to be the dominant ETD fragmentation pathway, in contrast to the preponderance of the products of glycosidic cleavages that has been observed in low- and high-energy CID. In ETD mass spectra, the presence of various product ions that originate from glycosidic cleavages, cross-ring cleavages and internal cleavages allow unambiguous identification of the structures of oligosaccharides. For the glycans cationized by adduction with different metals, the extent of CID fragmentation is cation-dependent, but the patterns of fragment ions are often very similar. However, we have established that both the dissociation pathways and the efficiencies vary significantly as a function of cation adduct under ETD conditions. The dissociation behaviors depend on the type of metal adduct. Magnesium adduction generally yields the best cleavage efficiency and provides more useful information than does adduction with any of the other metals that have been evaluated to date. According to our initial results reported herein, multiply-charged glycans subjected to ETD undergo radical-driven fragmentation processes accompanied by complex hydrogen migrations and rearrangements. Our proposed ETD mechanisms are based on model studies. More investigations remain to be carried out, involving a broader range of glycans that include more structural features. The fragmentation-driving features present in the selected samples, *e.g.*, the stereochemically favorable sites for metal adduction, and the amide substituents present in HexNAc and sialic acid residues, can also be found in many *N*- and *O*-linked glycans that can be released from glycoproteins or glycolipids. In summation, ETD shows considerable potential to become a very useful and powerful technique for detailed structural analysis of a wide variety of biological oligosaccharides.

Supplementary Material

Refer to Web version on PubMed Central for supplementary material.

Acknowledgments

This research is supported by NIH-NCRR grant No. P41 RR010888. The authors are grateful to Bruker Daltonics for loan of the AmaZon ETD instrument and to Prof. D. S. Newburg (Boston College) for his gift of the milk oligosaccharides. We thank Prof. C. Lin and X. Yu for helpful discussions.

References

1. Ohtsubo K, Marth JD. Glycosylation in cellular mechanisms of health and disease. Cell. 2006; 126:855–867. [PubMed: 16959566]
2. Varki, A.; Cummings, RD.; Esko, JD.; Freeze, HH.; Hart, GW.; Marth, J., editors. Essentials of Glycobiology. Cold Spring Harbor Laboratory Press; Cold Spring Harbor, New York: 1999.
3. Mutenda, KE.; Matthiesen, R. Analysis of carbohydrates by mass spectrometry. In: Matthiesen, R., editor. Mass Spectrometry Data Analysis in Proteomics. Humana Press; Totowa, New Jersey: 2006. p. 289
4. Xie, B.; Costello, CE. Carbohydrate structure determination by mass spectrometry. In: Cowman, MK.; Garg, HG.; Hales, CA., editors. Carbohydrate Chemistry, Biology and Medical Applications. Elsevier, Ltd; New York: 2008. p. 29
5. Ashline D, Singh S, Hanneman A, Reinhold V. Congruent strategies for carbohydrate sequencing. 1. Mining structural details by MSn. Anal Chem. 2005; 77:6250–6262. [PubMed: 16194086]
6. Reinhold VN, Reinhold BB, Costello CE. Carbohydrate molecular-weight profiling, sequence, linkage, and branching data - ES-MS and CID. Anal Chem. 1995; 67:1772–1784. [PubMed: 9306731]
7. Lemoine J, Fournet B, Despeyroux D, Jennings KR, Rosenberg R, d e Hoffmann E. Collision-induced dissociation of alkali-metal cationized and permethylated oligosaccharides-influence of the collision energy and of the collision gas for the assignment of linkage position. J Am Soc Mass Spectrom. 1993; 4:197–203.
8. Harvey DJ, Bateman RH, Green MR. High-energy collision-induced fragmentation of complex oligosaccharides ionized by matrix-assisted laser desorption/ionization mass spectrometry. J Mass Spectrom. 1997; 32:167–187. [PubMed: 9102200]
9. Adamson JT, Hakansson K. Electron capture dissociation of oligosaccharides ionized with alkali, alkaline earth, and transition metals. Anal Chem. 2007; 79:2901–2910. [PubMed: 17328529]
10. Zhao C, Xie B, Chan SY, Costello CE, O'Connor PB. Collisionally activated dissociation and electron capture dissociation provide complementary structural information for branched permethylated oligosaccharides. J Am Soc Mass Spectrom. 2008; 19:138–150. [PubMed: 18063385]
11. Wolff JJ, Chi LL, Linhardt RJ, Amster IJ. Distinguishing glucuronic from iduronic acid in glycosaminoglycan tetrasaccharides by using electron detachment dissociation. Anal Chem. 2007; 79:2015–2022. [PubMed: 17253657]
12. Wolff JJ, Amster IJ, Chi LL, Linhardt RJ. Electron detachment dissociation of glycosaminoglycan tetrasaccharides. J Am Soc Mass Spectrom. 2007; 18:234–244. [PubMed: 17074503]
13. Adamson JT, Hakansson K. Electron detachment dissociation of neutral and sialylated oligosaccharides. J Am Soc Mass Spectrom. 2007; 18:2162–2172. [PubMed: 17962039]
14. Syka JEP, Coon JJ, Schroeder MJ, Shabanowitz J, Hunt DF. Peptide and protein sequence analysis by electron transfer dissociation mass spectrometry. Proc Natl Acad Sci U S A. 2004; 101:9528–9533. [PubMed: 15210983]
15. Wiesner J, Premsler T, Sickmann A. Application of electron transfer dissociation (ETD) for the analysis of posttranslational modifications. Proteomics. 2008; 8:4466–4483. [PubMed: 18972526]
16. Molina H, Horn DM, Tang N, Mathivanan S, Pandey A. Global proteomic profiling of phosphopeptides using electron transfer dissociation tandem mass spectrometry. Proc Natl Acad Sci U S A. 2007; 104:2199–2204. [PubMed: 17287340]
17. Hogan JM, Pitteri SJ, Chrisman PA, McLuckey SA. Complementary structural information from a tryptic *N*-linked glycopeptide via electron transfer ion/ion reactions and collision-induced dissociation. J Proteome Res. 2005; 4:628–632. [PubMed: 15822944]

18. March RE. Quadrupole ion trap mass spectrometry: a view at the turn of the century. Int J Mass Spectrom. 2000; 200:285–312.
19. Lapadula AJ, Hatcher PJ, Hanneman AJ, Ashline DJ, Zhang HL, Reinhold VN. Congruent strategies for carbohydrate sequencing. 3. OSCAR: An algorithm for assigning oligosaccharide topology from MS^n data. Anal Chem. 2005; 77:6271–6279. [PubMed: 16194088]
20. Viseux N, de Hoffmann E, Domon B. Structural assignment of permethylated oligosaccharide subunits using sequential tandem mass spectrometry. Anal Chem. 1998; 70:4951–4959. [PubMed: 9852781]
21. Viseux N, de Hoffmann E, Domon B. Structural analysis of permethylated oligosaccharides by electrospray tandem mass spectrometry. Anal Chem. 1997; 69:3193–3198. [PubMed: 9271064]
22. Sheeley DM, Reinhold VN. Structural characterization of carbohydrate sequence, linkage, and branching in a quadrupole ion trap mass spectrometer: Neutral oligosaccharides and *N*-linked glycans. Anal. Chem. 1998; 70:3053–3059.
23. Ashline DJ, Lapadula AJ, Liu YH, Lin M, Grace M, Pramanik B, Reinhold VN. Carbohydrate structural isomers analyzed by sequential mass spectrometry. Anal Chem. 2007; 79:3830–3842. [PubMed: 17397137]
24. Carroll JA, Willard D, Lebrilla CB. Energetics of cross-ring cleavages and their relevance to the linkage determination of oligosaccharides. Anal Chim Acta. 1995; 307:431–447.
25. Harvey DJ. Ionization and collision-induced fragmentation of *N*-linked and related carbohydrates using divalent canons. J. Am. Soc. Mass Spectrom. 2001; 12:926–937.
26. Hofmeister GE, Zhou Z, Leary JA. Linkage position determination in lithium-cationized disaccharides-tandem mass-spectrometry and semiempirical calculations. J Am Chem Soc. 1991; 113:5964–5970.
27. Harvey DJ. Collision-induced fragmentation of underivatized *N*-linked carbohydrates ionized by electrospray. J Mass Spectrom. 2000; 35:1178–1190. [PubMed: 11110090]
28. Fura A, Leary JA. Differentiation of Ca^{2+}-coordinated and Mg^{2+}-coordinated branched trisaccharide isomers-an electrospray-ionization and tandem mass-spectrometry study Anal. Chem. 1993; 65:2805–2811.
29. Cancilla MT, Penn SG, Carroll JA, Lebrilla CB. Coordination of alkali metals to oligosaccharides dictates fragmentation behavior in matrix-assisted laser desorption/ ionization Fourier transform mass spectrometry. J Am Chem Soc. 1996; 118:6736–6745.
30. Zaia J. Mass spectrometry of oligosaccharides. Mass Spectrom Rev. 2004; 23:161–227. [PubMed: 14966796]
31. Zaia J. Mass Spectrometry and the emerging field of glycomics. Chem Biol. 2008; 15:881–892. [PubMed: 18804025]
32. Lemoine J, Chirat F, Domon B. Structural analysis of derivatized oligosaccharides using post-source decay matrix-assisted laser desorption/ionization mass spectrometry. J Mass Spectrom. 1996; 31:908–912. [PubMed: 8799317]
33. Mechref Y, Kang P, Novotny MV. Differentiating structural isomers of sialylated glycans by matrix-assisted laser desorption/ionization time-of-flight/time-of-flight tandem mass spectrometry. Rapid Commun Mass Spectrom. 2006; 20:1381–1389. [PubMed: 16557638]
34. Sible EM, Brimmer SP, Leary JA. Interaction of first row transition metals with alpha 1–3, alpha 1–6 mannotriose and conserved trimannosyl core oligosaccharides: A comparative electrospray ionization study of doubly and singly charged complexes. J Am Soc Mass Spectrom. 1997; 8:32–42.
35. Sinnott, ML. Carbohydrate chemistry and biochemistry. 1. The Royal Society of Chemistry; Cambridge, UK: 2007.
36. Garcia BA, Gin DY. Dehydrative glycosylation with activated diphenyl sulfonium reagents. Scope, mode of C(1)-hemiacetal activation, and detection of reactive glycosyl intermediates. J Am Chem Soc. 2000; 122:4269–4279.
37. Costello CE, Contado-Miller JM, Cipollo JF. A glycomics platform for the analysis of permethylated oligosaccharide alditols. J Am Soc Mass Spectrom. 2007; 18:1799–1812. [PubMed: 17719235]

38. Ciucanu I, Kerek F. A simple and rapid method for the permethylation of carbohydrates. Carbohydr Res. 1984; 131:209–217.

39. Ciucanu I, Costello CE. Elimination of oxidative degradation during the per-O-methylation of carbohydrates. J Am Chem Soc. 2003; 125:16213–16219. [PubMed: 14692762]

40. Swaney DL, McAlister GC, Wirtala M, Schwartz JC, Syka JEP, Coon JJ. Supplemental activation method for high-efficiency electron-transfer dissociation of doubly protonated peptide precursors. Anal Chem. 2007; 79:477–485. [PubMed: 17222010]

41. Domon B, Costello CE. A systematic nomenclature for carbohydrate fragmentations in FAB-MSMS spectra of glycoconjugates. Glycoconjugate J. 1988; 5:397–409.

42. Hunt DF, Stafford GC, Crow FW, Russell JW. Pulsed positive-negative-ion chemical ionization mass spectrometry. Anal Chem. 1976; 48:2098–2105.

43. Gunawardena HP, He M, Chrisman PA, Pitteri SJ, Hogan JM, Hodges BDM, McLuckey SA. Electron transfer versus proton transfer in gas-phase ion/ion reactions of polyprotonated peptides. J Am Chem Soc. 2005; 127:12627–12639. [PubMed: 16144411]

44. Gyurcsik B, Nagy L. Carbohydrates as ligands: coordination equilibria and structure of the metal complexes. Coord Chem Rev. 2000; 203:81–149.

45. Zheng YJ, Ornstein RL, Leary JA. A density functional theory investigation of metal ion binding sites in monosaccharides. Theochem-J Mol Struct. 1997; 389:233–240.

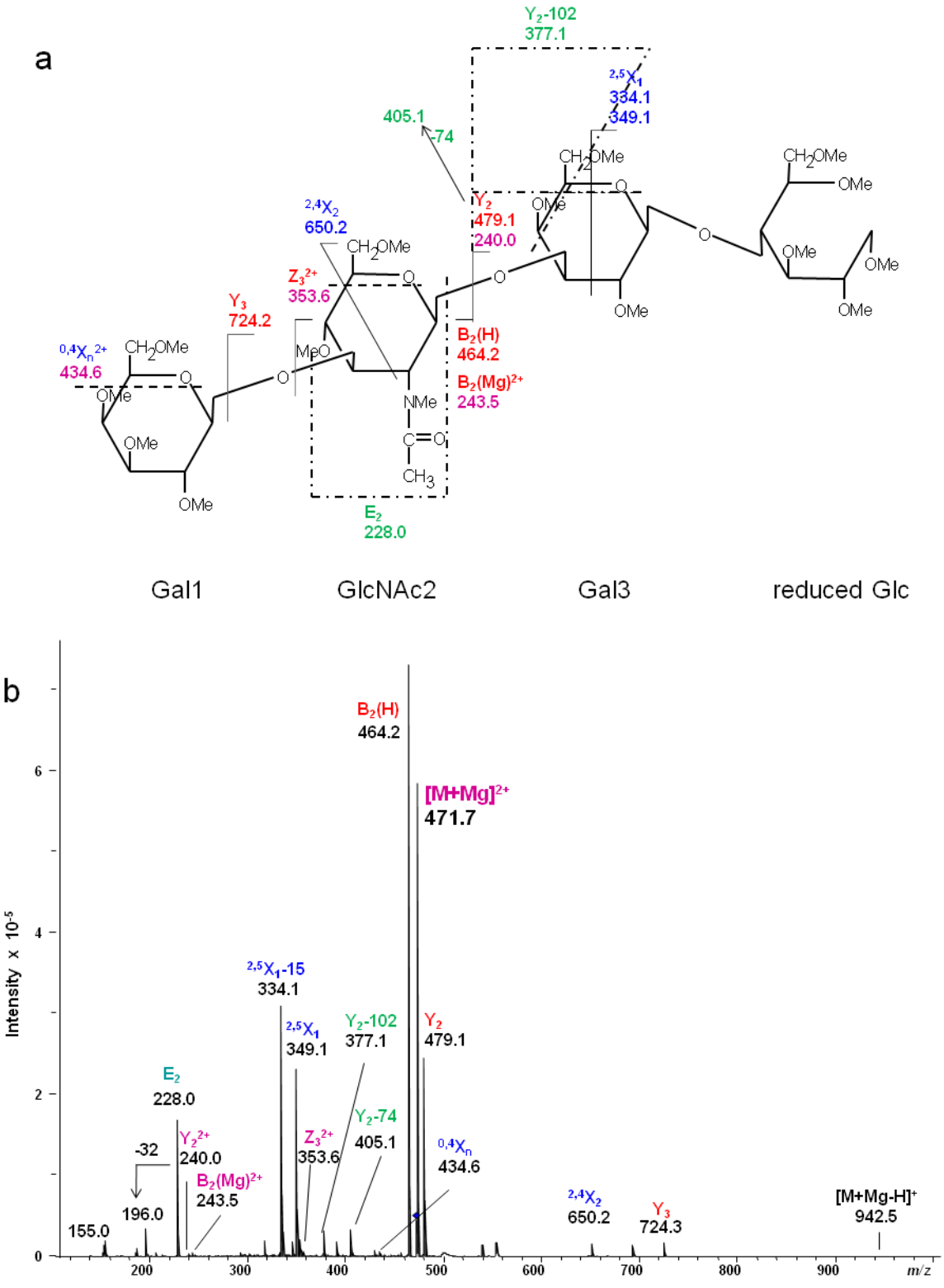

Figure 1.

(a) CID MS/MS fragmentation of reduced and permethylated LNT [M + Mg]$^{2+}$ *m/z* 471.7.
(b) CID MS/MS spectrum. In this figure and all other figures, the ions that result from

glycosidic cleavages have been labeled in red; those that originate from cross-ring cleavages have been labeled in blue, and those from internal cleavages, in green. The peaks labeled in purple represent doubly-charged ions.

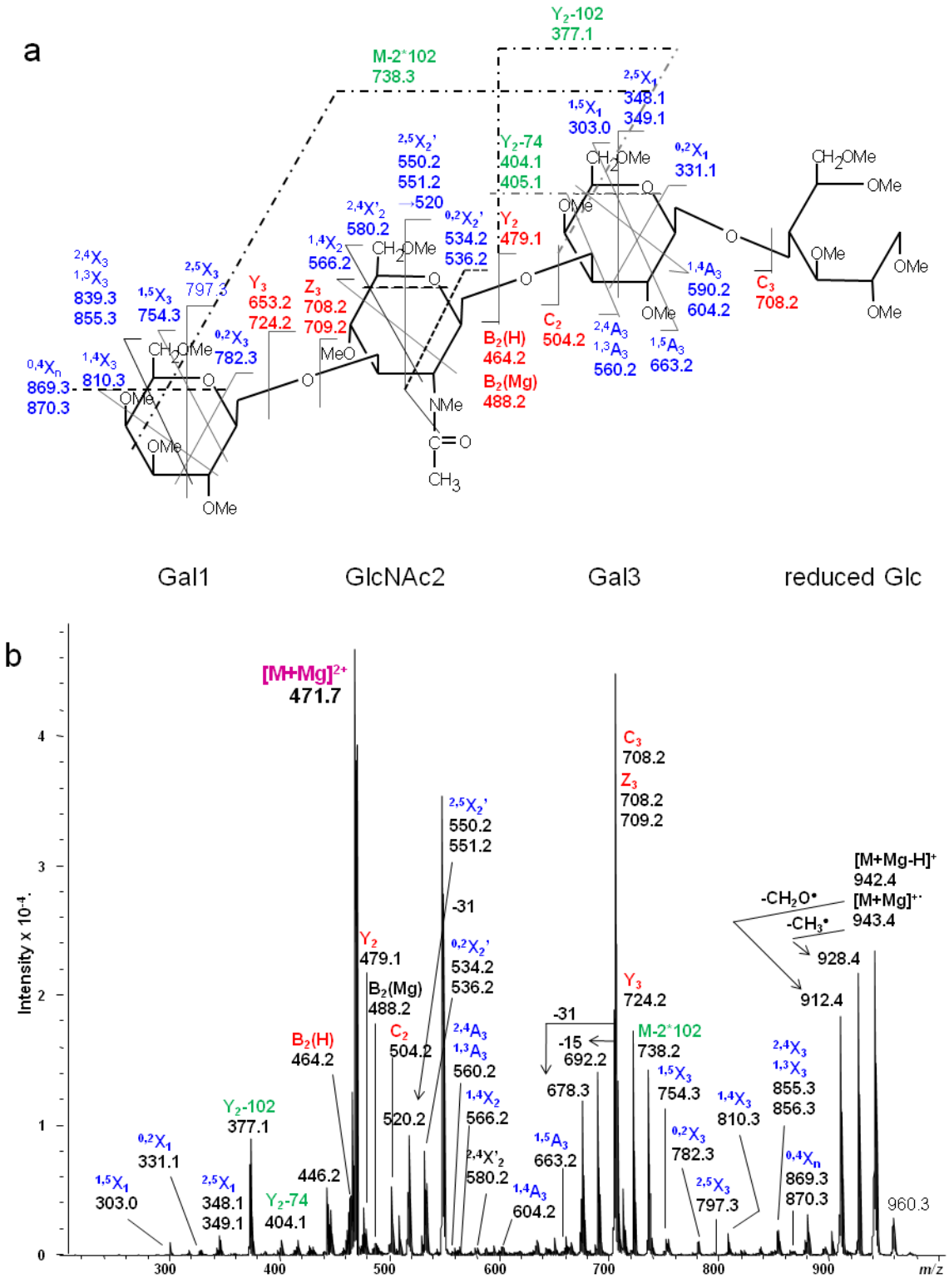

Figure 2.

(a) ETD MS/MS fragmentation of reduced and permethylated LNT $[M + Mg]^{2+}$ *m/z* 471.7.
(b) ETD MS/MS spectrum.

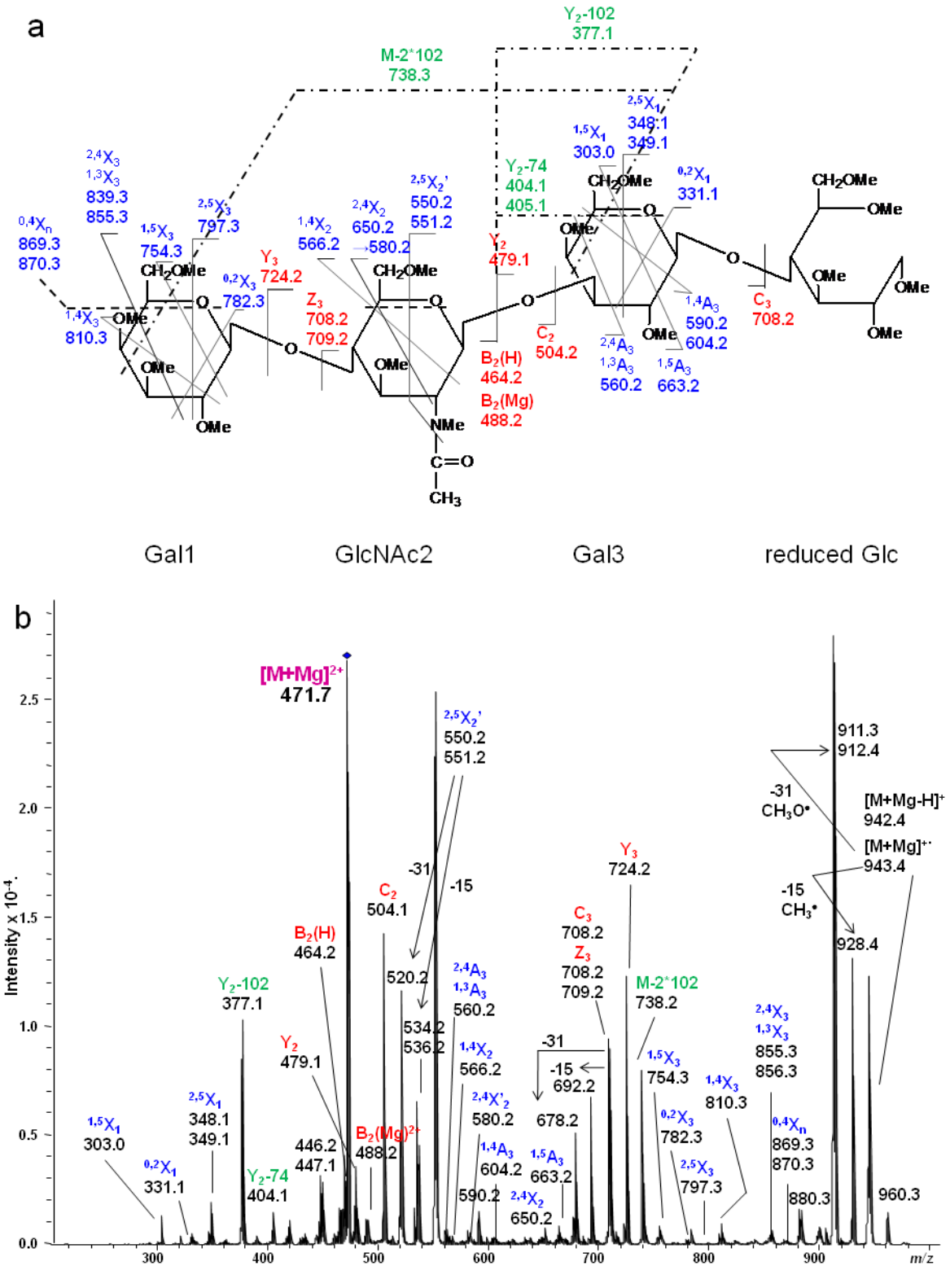

Figure 3.

(a) ETD MS/MS fragmentation of reduced and permethylated LNnT [M + Mg]$^{2+}$ *m/z* 471.7.
(b) ETD MS/MS spectrum.

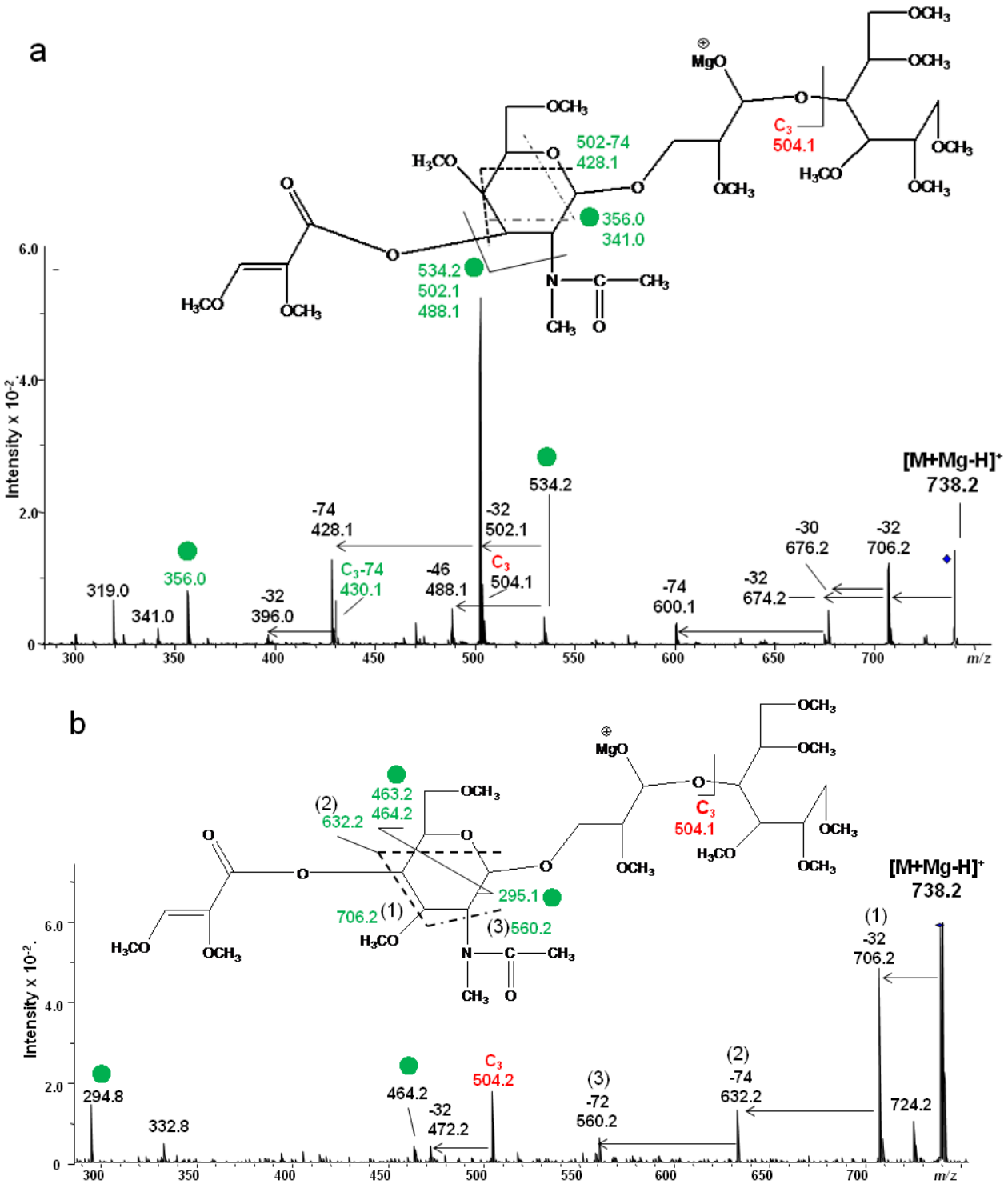

Figure 4.

ETD/CID MS^3 fragmentation and CID MS^3 spectra of $[M + Mg - H]^+$ *m/z* 738.2 generated *via* ETD of $[M + Mg]^{2+}$ of (a) reduced and permethylated LNT and (b) reduced and permethylated LNnT.

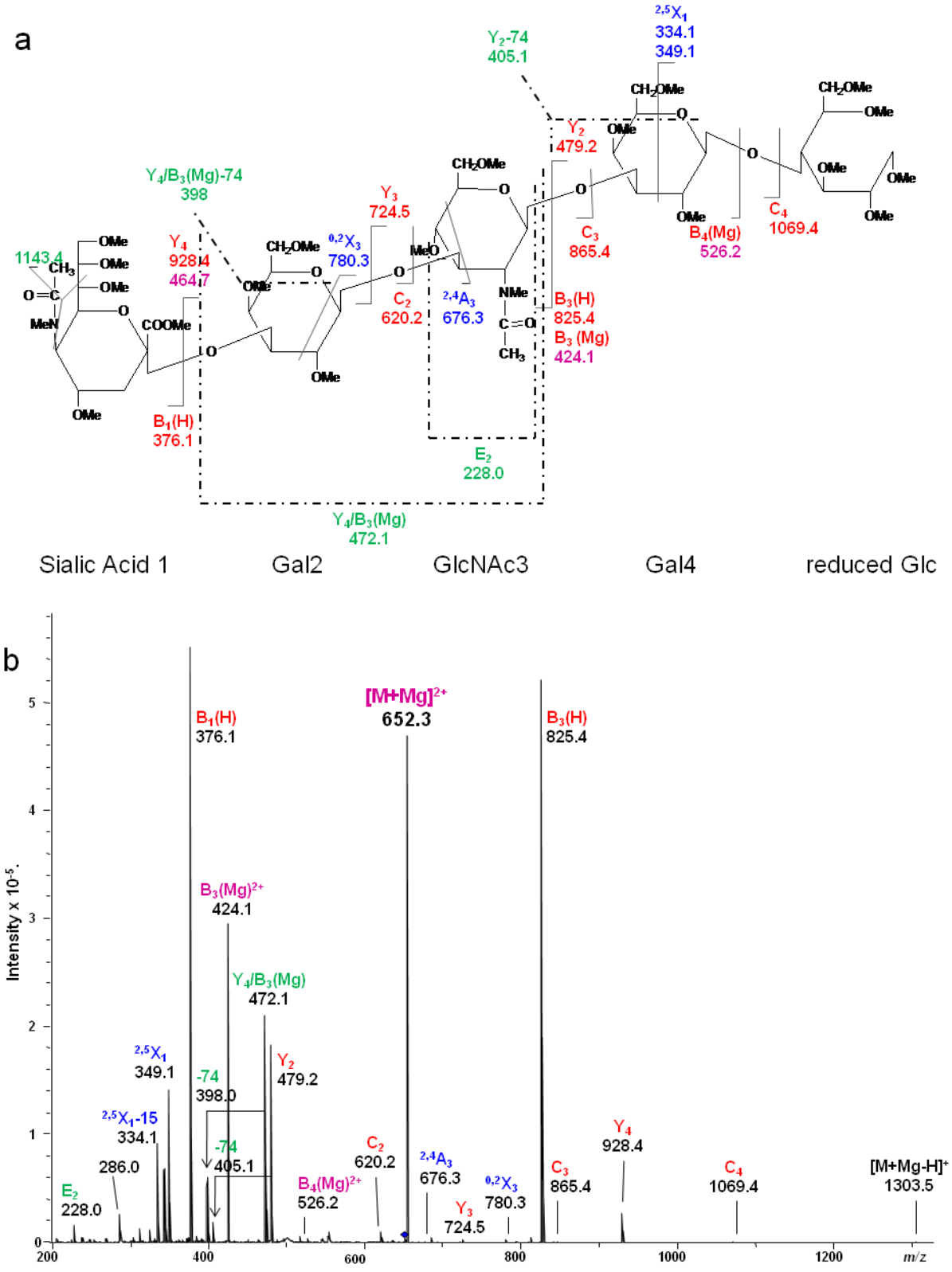

Figure 5.

CID MS/MS (a) fragmentation and (b) spectrum of reduced and permethylated LSTa $[M + Mg]^{2+}$ *m/z* 652.3.

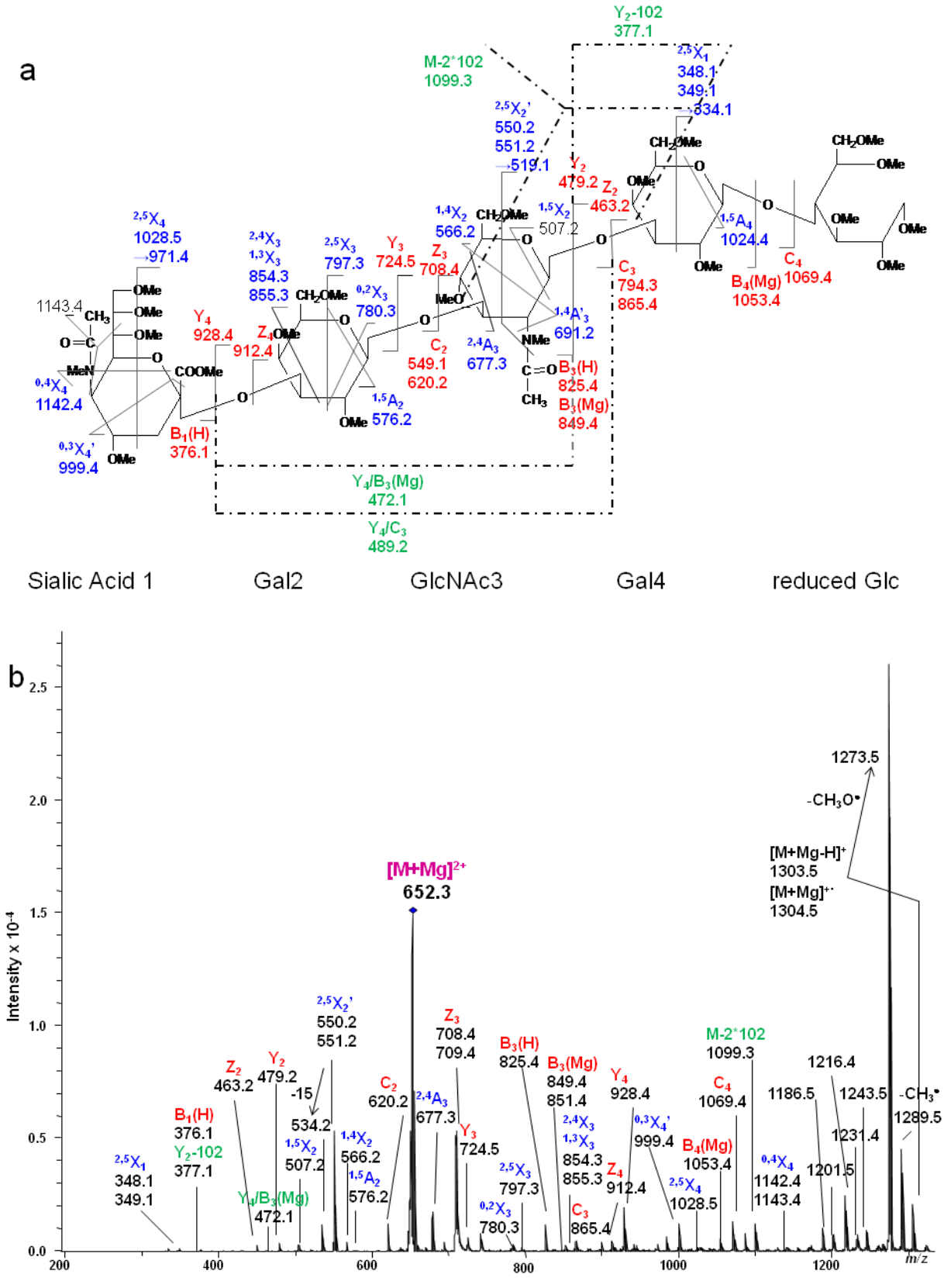

Figure 6.
ETD MS/MS (a) fragmentation and (b) spectrum of reduced and permethylated LSTa $[M + Mg]^{2+}$ *m/z* 652.3.

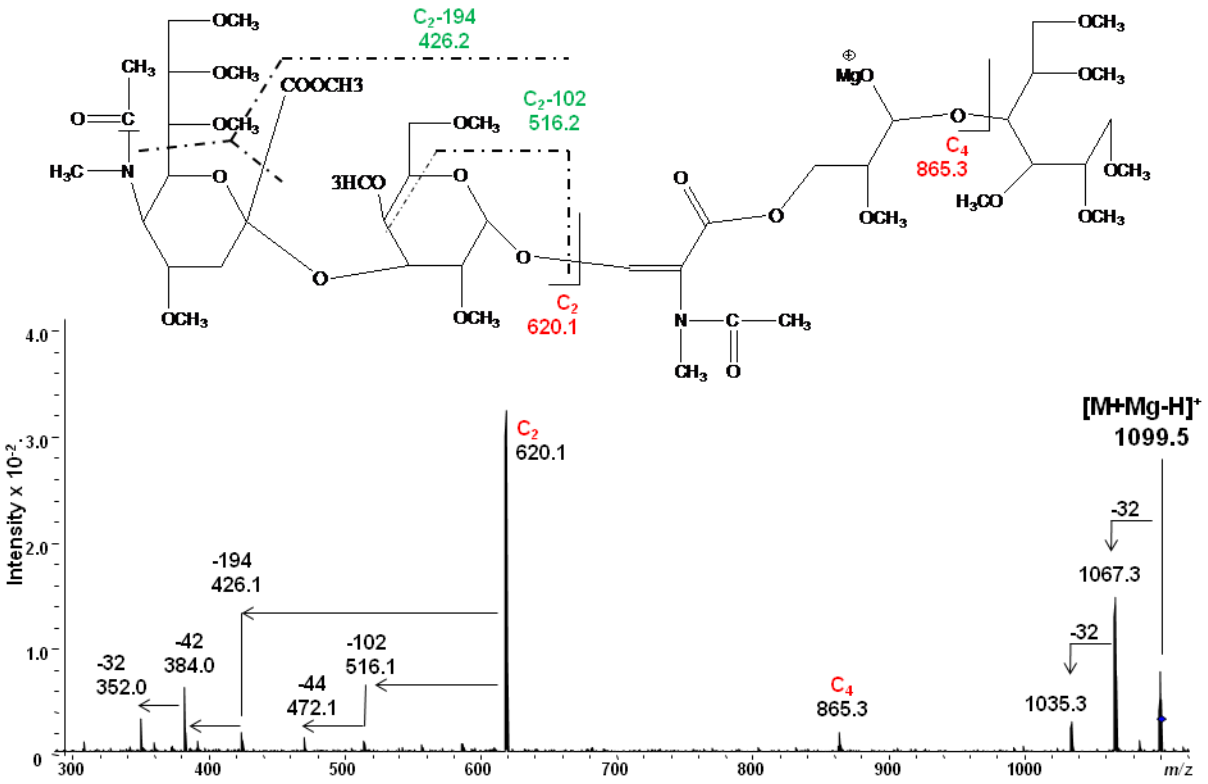

Figure 7.

ETD/CID MS^3 fragmentation and CID MS^3 spectrum of the product ion $[M + Mg - H]^+$ *m/z* 1099.5 that is generated *via* loss of H^+ and two eliminations of $CH_3OCH{=}CHCH_2OCH_3$ (2x102 Da) in the ETD MS/MS spectrum of the $[M + Mg]^{2+}$ of reduced and permethylated LSTa

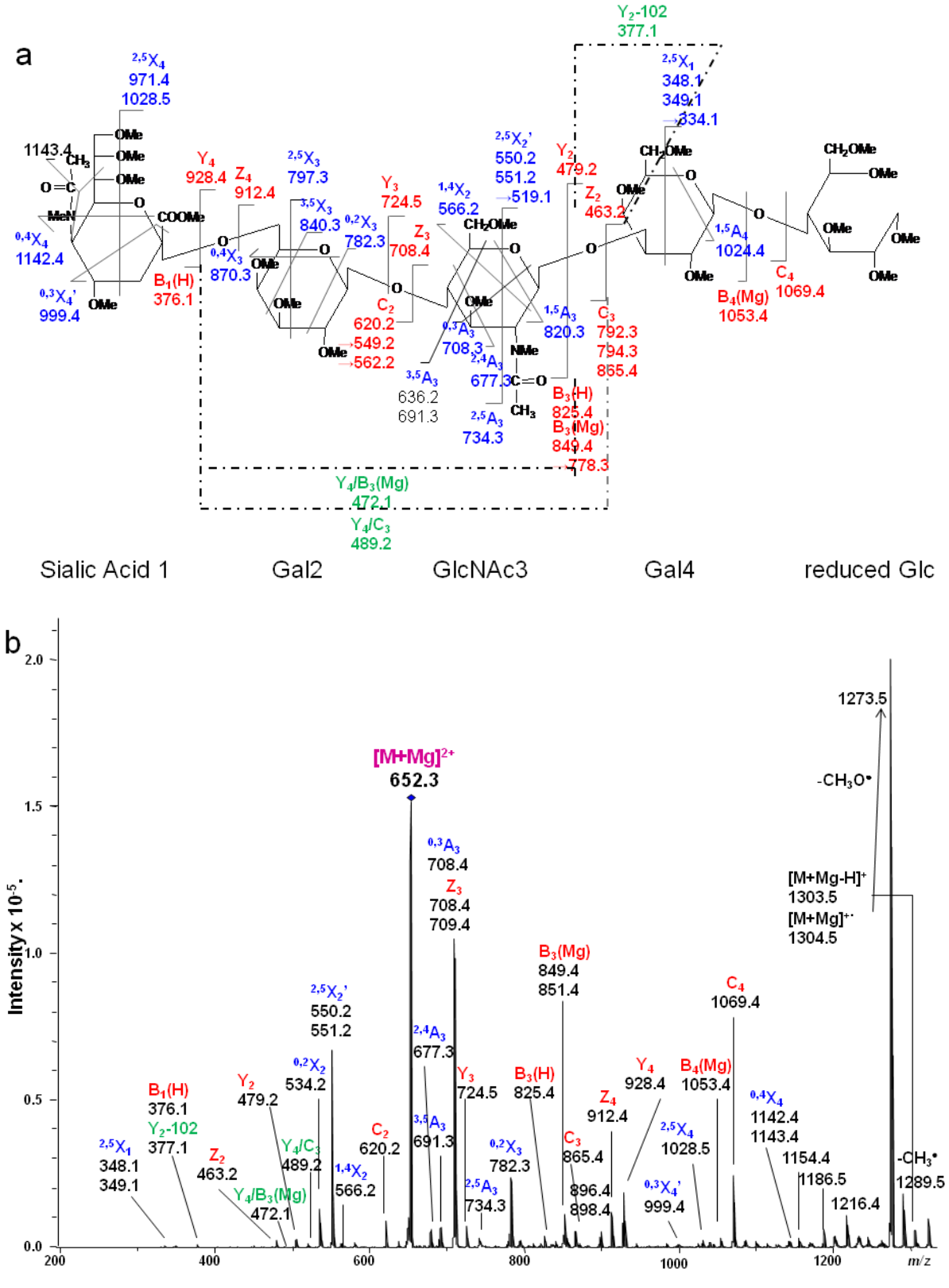

Figure 8.

ETD MS/MS (a) fragmentation and (b) spectrum of reduced and permethylated LSTc $[M + Mg]^{2+}$ *m/z* 652.3. Fragments between *m/z* 1142.2 and 1216.4 are attributed to cleavages within the sialic acid residue.

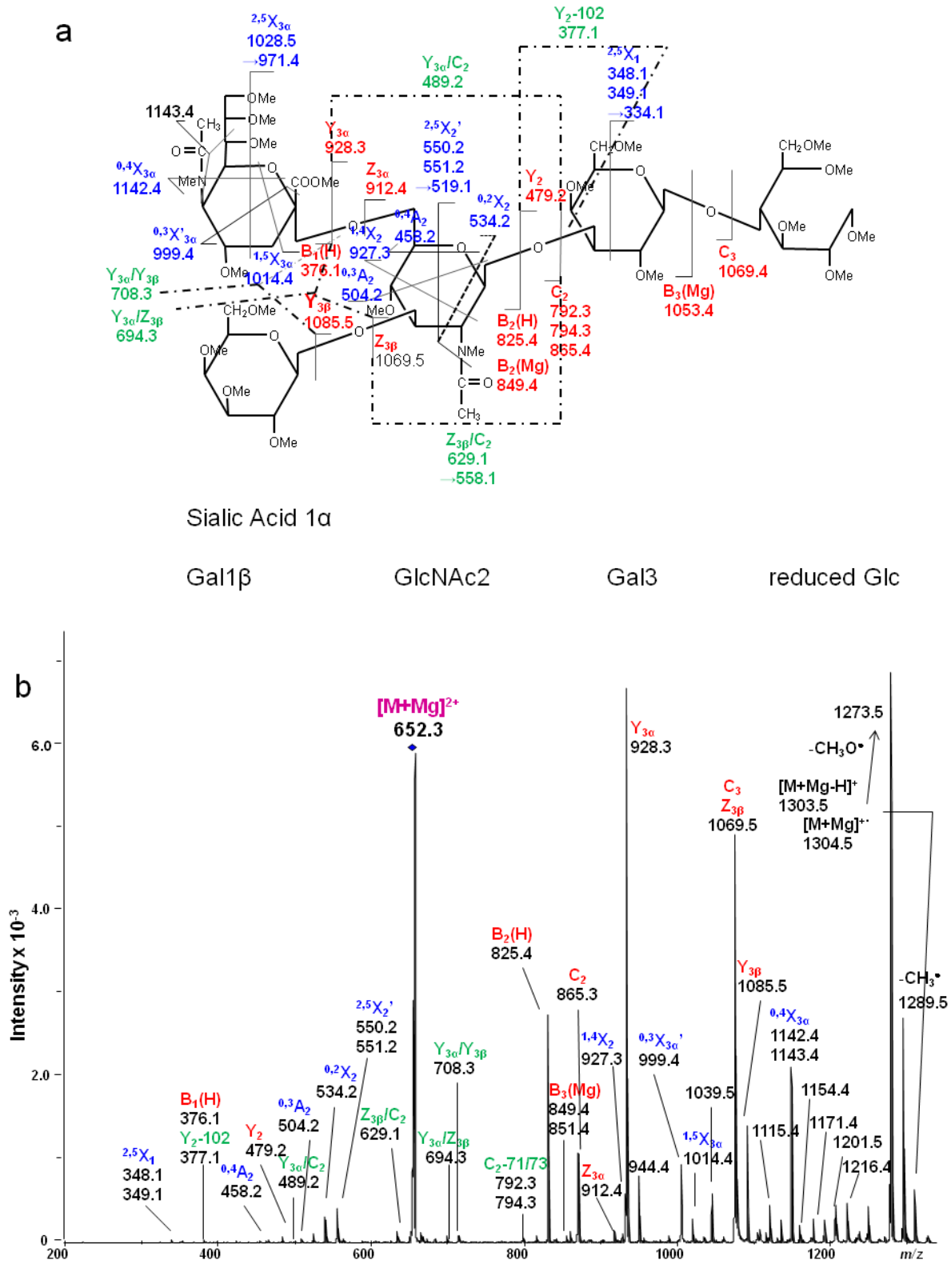

Figure 9.

ETD MS/MS (a) fragmentation and (b) spectrum of reduced and permethylated LSTb [M + Mg]$^{2+}$ *m/z* 652.3. Fragments between *m/z* 1115.4 and 1216.4 are attributed to cleavages within the sialic acid residue.

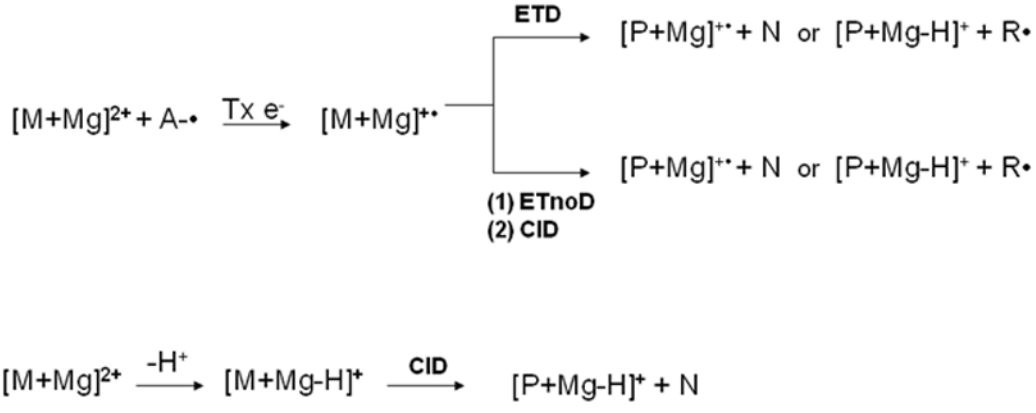

A = anion, M = neutral molecule, N = neutral product, P = product observed as ion

Scheme 1.

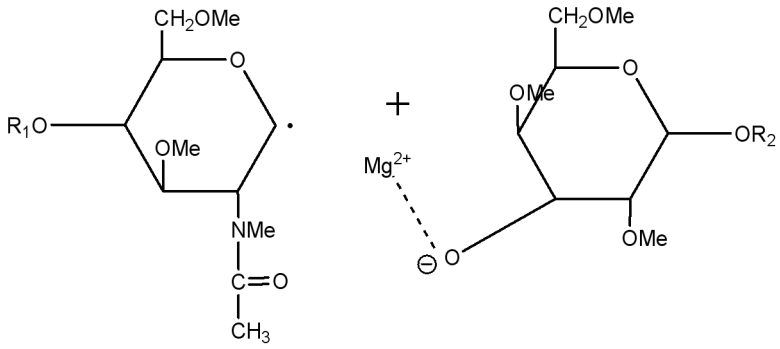

Scheme 2.
Y-type ETD ion and neutral radical

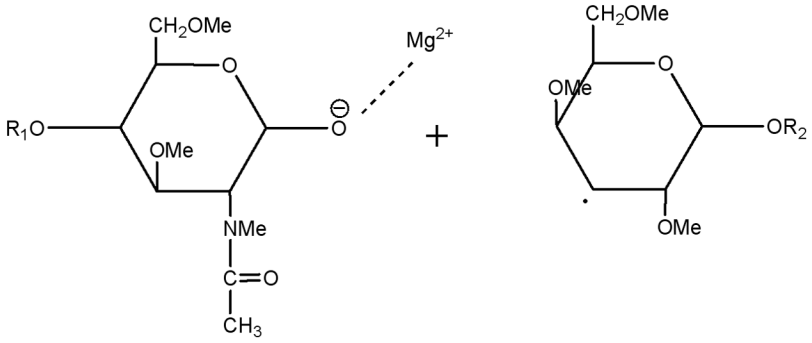

Scheme 3.
C-type ETD product ion and neutral radical

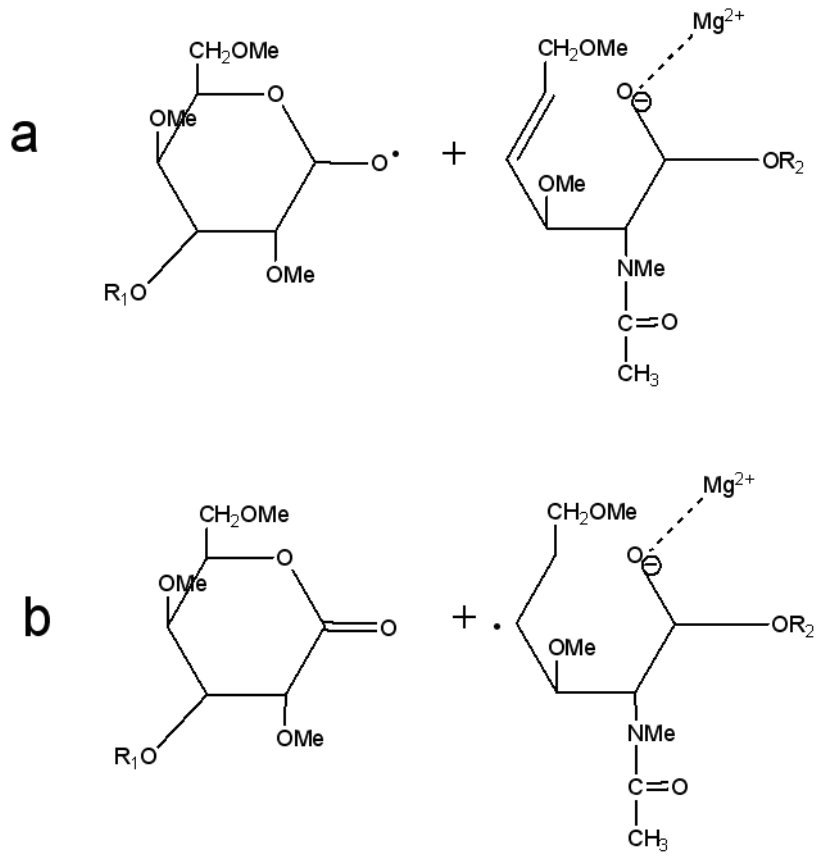

Scheme 4.
(a) Singly-charged even-electron Z-type ions and (b) singly-charged odd-electron Z-type ions

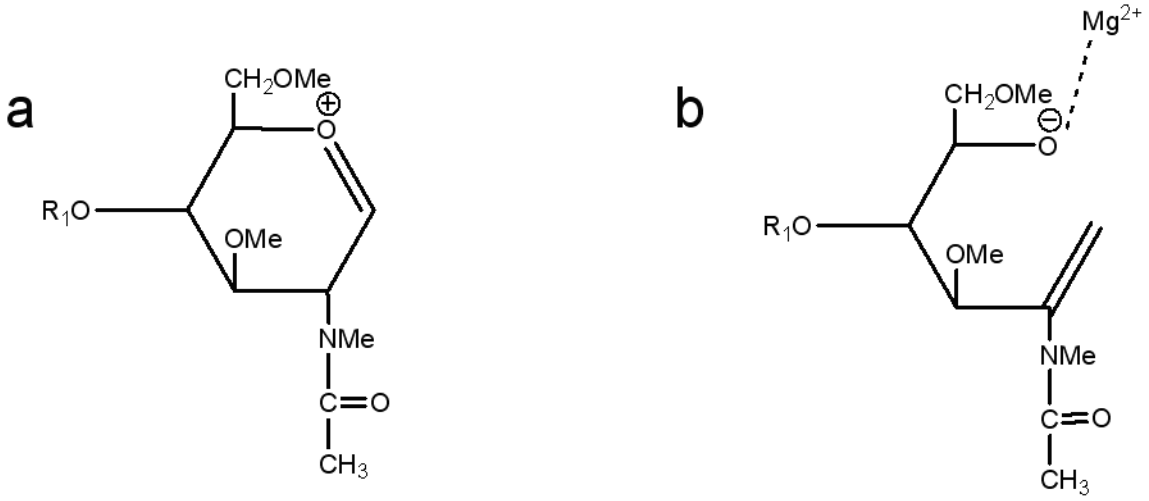

Scheme 5.
Suggested structures of (a) $[B_n(H)]^+$ and (b) $[B_n(Mg)+2H]^+$- ions.

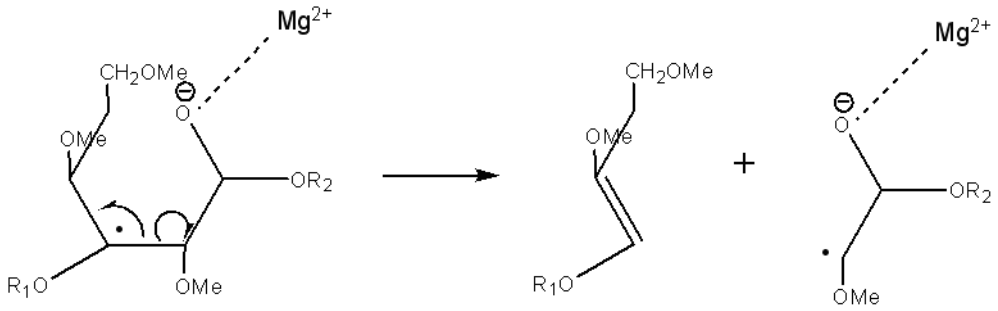

Scheme 6.
Suggested structures of $^{2,5}X_n$ ETD product ions and neutral loss

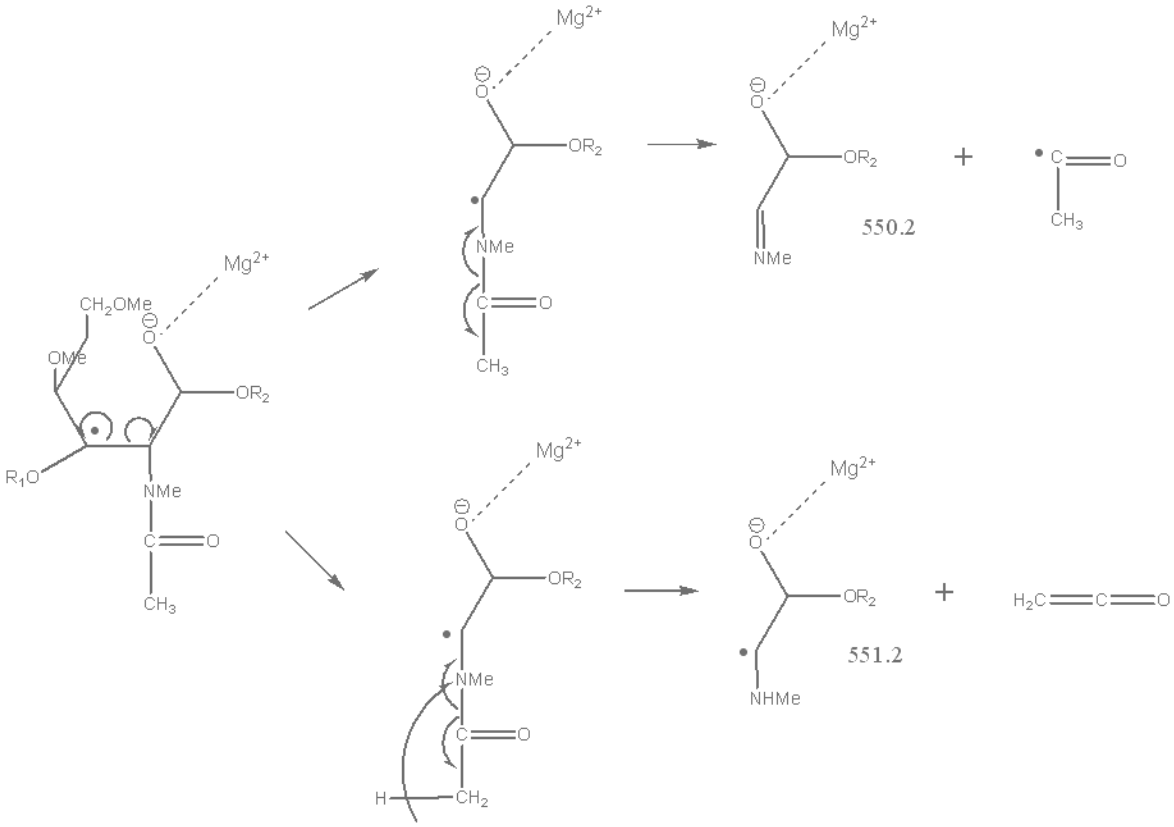

Scheme 7.
Suggested route for formation of $^{2,5}X_n'$ ETD product ions

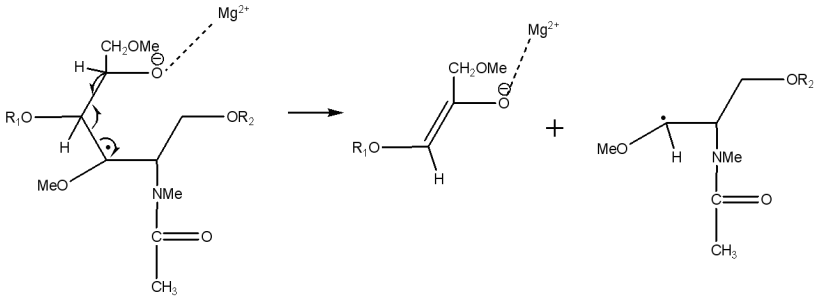

Scheme 8.
Suggested structures of $^{0,3}A_n$ ETD product ion and neutral radical